ELECTROMAGNETISM

10.1126/sciadv.1500916

Multiferroicity and skyrmions carrying electric polarization in GaV_4S_8

Eugen Ruff,[1]* Sebastian Widmann,[1] Peter Lunkenheimer,[1] Vladimir Tsurkan,[1,2] Sandor Bordács,[3] Istvan Kézsmárki,[1,3] Alois Loidl[1]

Skyrmions are whirl-like topological spin objects with high potential for future magnetic data storage. A fundamental question that is relevant to both basic research and application is whether ferroelectric (FE) polarization can be associated with skyrmions' magnetic texture and whether these objects can be manipulated by electric fields. We study the interplay between magnetism and electric polarization in the lacunar spinel GaV_4S_8, which undergoes a structural transition associated with orbital ordering at 44 K and reveals a complex magnetic phase diagram below 13 K, including ferromagnetic, cycloidal, and Néel-type skyrmion lattice (SkL) phases. We found that the orbitally ordered phase of GaV_4S_8 is FE with a sizable polarization of ~1 μC/cm^2. Moreover, we observed spin-driven excess polarizations in all magnetic phases; hence, GaV_4S_8 hosts three different multiferroic phases with coexisting polar and magnetic order. These include the SkL phase, where we predict a strong spatial modulation of FE polarization close to the skyrmion cores. By taking into account the crystal symmetry and spin patterns of the magnetically ordered phases, we identify exchange striction as the main microscopic mechanism behind the spin-driven FE polarization in each multiferroic phase. Because GaV_4S_8 is unique among known SkL host materials owing to its polar crystal structure and the observed strong magnetoelectric effect, this study is an important step toward the nondissipative electric field control of skyrmions.

INTRODUCTION

In recent years, magnetic skyrmions—whirl-like spin textures with a nontrivial topology and a typical size of 1 to 100 nm—have attracted tremendous interest from the academic and technological fields (*1*–*4*). Besides the formation of individual skyrmions, these objects can be arranged in skyrmion lattices (SkLs), representing a new form of magnetic order (*1*, *2*). Owing to their topology and nanometric size, skyrmions are stable against external perturbations (*5*). Because each skyrmion is associated with a quantized magnetic flux, its creation and annihilation must be related to singular magnetic defects, which can be regarded as analogs of magnetic monopoles (*6*, *7*). Metallic chiral magnets, where skyrmions can be moved over macroscopic distances by low electrical currents, can be exploited for spintronic applications such as racetrack memories (*3*). In addition, insulating skyrmion host materials have been recently discovered (*8*, *9*), raising the possibility of multiferroic behavior in these systems. Multiferroicity, the coexistence of magnetic and polar orders, may favor the manipulation of magnetic patterns via electrical fields without Joule heating (*10*, *11*). Such nondissipative electronic control of nanometric magnetic objects is very promising for applications in new-generation magnetic memories and spintronic devices. Indeed, shortly after the first observation of skyrmions in multiferroic Cu_2OSeO_3 (*8*), electric field control of SkLs in this compound was also demonstrated (*12*, *13*). The dielectric response and emergent electrodynamics of skyrmions have also been extensively studied, experimentally and theoretically, in both itinerant and insulating magnets (*5*, *7*, *14*–*18*).

Lacunar spinels, ternary chalcogenides of composition AM_4X_8 (A = Ga and Ge; M = V, Mo, Nb, and Ta; X = S and Se), represent an interesting class of transition metal compounds with the weakly linked molecular units cubane $(M_4X_4)^{n+}$ and tetrahedral $(AX_4)^{n-}$ as structural building blocks (*19*–*22*). Recently, a plethora of correlation effects has been reported for AM_4X_8 lacunar spinels, including pressure-induced superconductivity (*23*), bandwidth-controlled metal-to-insulator transition (*24*, *25*), large negative magnetoresistance (*26*), a two-dimensional topological insulating state (*27*), resistive switching through electric field–induced transition (*28*–*30*), emergence of orbitally driven ferroelectricity (*31*), and an extended Néel-type SkL phase (*9*).

The vanadium-derived lacunar spinel GaV_4S_8 is a magnetic semiconductor with a noncentrosymmetric cubic structure (point symmetry group T_d) at room temperature (*32*, *33*). It consists of a network of weakly coupled $(V_4S_4)^{5+}$ cubane units forming a face-centered cubic (fcc) lattice separated by $(GaS_4)^{5-}$ tetrahedra. Each vanadium V_4 cluster carries a single local spin S = ½ (*33*). GaV_4S_8 undergoes a cubic-to-rhombohedral structural phase transition at T_{JT} = 44 K and magnetic ordering at T_C = 13 K (*22*, *34*, *35*). The structural phase transition has been identified as a Jahn-Teller–derived orbital ordering characterized by the elongation of the V_4 tetrahedra along one of the four crystallographic ⟨111⟩ directions (*33*, *36*) (inset to Fig. 1B), leading to a low-temperature rhombohedral C_{3v} point group symmetry (*32*, *33*). Kézsmárki *et al.* (*9*) revealed a complex magnetic phase diagram of GaV_4S_8 with cycloidal and SkL phases embedded within the ferromagnetic (FM) state. SkLs have recently been observed in various magnets with chiral structures (*1*, *2*, *8*, *37*). In GaV_4S_8, novel Néel-type skyrmions, which are composed of spin cycloids and carry a monopole moment (*38*), have been identified (*9*).

Here we report a detailed study of the ferroelectric (FE) properties of GaV_4S_8 as a function of temperature and magnetic field, supplemented by measurements of specific heat and magnetic susceptibility. We provide experimental evidence for the onset of FE order with a sizable polarization at the Jahn-Teller transition. In addition, we find that FE polarization is enhanced when magnetic phase boundaries are crossed,

[1]Experimental Physics V, Center for Electronic Correlations and Magnetism, University of Augsburg, Augsburg 86135, Germany. [2]Institute of Applied Physics, Academy of Sciences of Moldova, Chisinau MD-2028, Republic of Moldova. [3]Department of Physics, Budapest University of Technology and Economics and MTA-BME Lendület Magneto-Optical Spectroscopy Research Group, Budapest 1111, Hungary.
*Corresponding author. E-mail: eugen.ruff@physik.uni-augsburg.de

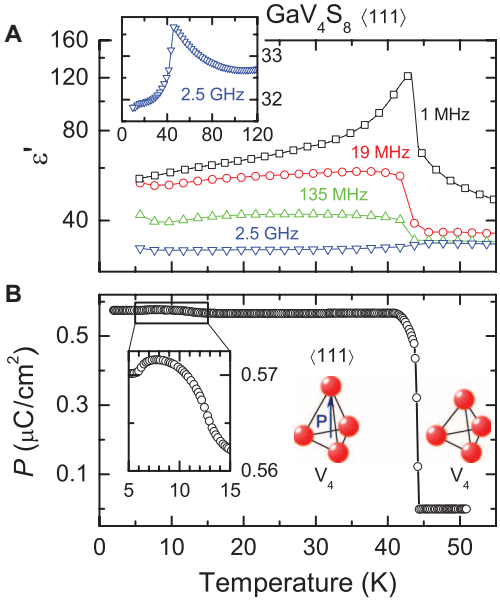

Fig. 1. Characterization of dielectric properties. (**A**) Real part of the dielectric constant ε′ measured at frequencies between 1 MHz (open squares) and 2.5 GHz (open triangles down). The electric field *E* was applied parallel to the crystallographic ⟨111⟩ direction. (**Inset**) An enlarged view of the measurements at 2.5 GHz. (**B**) Electric polarization *P* versus temperature measured parallel to the ⟨111⟩ direction. The elongation of the V_4 units along the ⟨111⟩ direction is schematically indicated and contrasted with the orbitally degenerate high-temperature phase. (**Inset**) Excess polarization at the onset of magnetic order on an enlarged scale.

leading to different polarizations in the collinear FM, cycloidal, and SkL phases. On the basis of spin patterns in the three magnetically ordered phases and the symmetry of V_4–V_4 bonds in the rhombohedral phase, we identify exchange striction as the main microscopic origin of all spin-driven FE polarizations in GaV_4S_8 and estimate the corresponding exchange striction parameters from the variation of polarizations between the different magnetic phases.

RESULTS

Sample characterization

We characterized the GaV_4S_8 single crystal studied in the present report by measurements of magnetic susceptibility and specific heat (for details, see fig. S1). Both structural and magnetic phase transitions are clearly manifested in the anomalies of these thermodynamic quantities at T_{JT} = 44.0 K and T_C = 12.7 K, respectively. The structural phase transition, as seen in susceptibility and dielectric measurements, is accompanied by a hysteresis loop on heating and cooling, similar to the findings for GeV_4S_8 (*39*) (figs. S2 and S3).

Figure 1A shows the temperature dependence of the real part of the dielectric constant measured at selected frequencies. A significant anomaly appears at the Jahn-Teller transition, which substantially depends on frequency. The strong suppression of the maximum dielectric constant at the structural phase transition resembles the behavior commonly observed in order-disorder ferroelectrics (*40*). At high temperatures and low frequencies, the dielectric constant is strongly influenced by extrinsic Maxwell-Wagner–like contributions, which arise from contact and surface effects and yield values >10^3 at room temperature (*41*, *42*). Such extrinsic contributions to the low-frequency dielectric constant are still present at T_{JT}; hence, we restrict ourselves to relatively high frequencies where intrinsic dielectric constants are measured and Maxwell-Wagner contributions are shifted to temperatures higher than 100 K (fig. S4). When approaching the Jahn-Teller transition from the cubic phase, the increase in the dielectric constant, as measured at 2.5 GHz and as documented in Fig. 1A (inset), suggests the presence of strong polar fluctuations. It seems quite natural to correlate these polar fluctuations with orbital fluctuations via a dynamic Jahn-Teller effect. In this case, the primary-order parameter is the Jahn-Teller distortion, which gives rise to FE polarization due to the noncentrosymmetric crystal structures of the low-temperature and high-temperature phases. The onset of magnetic order is hardly visible in the temperature dependence of the dielectric constant. The temperature dependence of the dielectric constant in FE and isostructural GeV_4S_8 also shows a very unusual behavior (*31*).

In GaV_4S_8, the FE polarization along the ⟨111⟩ direction (determined from pyrocurrent measurements; fig. S1B) abruptly appears at the structural transition (Fig. 1B), in agreement with the observed sharp anomaly in heat capacity (Supplementary Materials). The polarization saturates somewhat below 0.6 μC/cm^2, which is significantly larger than the polarization in spin-driven multiferroics (*43*–*45*) but is still a factor of 50 lower than that in canonical perovskite ferroelectrics (*46*). This value is close to the FE polarization found in the related lacunar spinel GeV_4S_8 (*31*). Figure 1B shows the elongation of the vanadium tetrahedra along the ⟨111⟩ direction driven by the concomitant orbital order originally proposed by Pocha *et al.* (*33*) and Nakamura *et al.* (*36*), which is responsible for the macroscopic polarization. According to this scenario, GaV_4S_8 is an orbital order–driven FE, where the lifting of orbital degeneracy at the Jahn-Teller transition induces FE polarization.

A closer inspection of Fig. 1B reveals additional features related to magnetic phase transitions. The inset to Fig. 1B provides an enlarged view of low-temperature polarization, which shows an increase upon entry to the cycloidal phase at 12.7 K and a small decrease close to 6 K when the low-temperature FM order is finally established (*9*). This finding documents that, in GaV_4S_8, an excess spin-driven polarization on the order of 100 μC/m^2—in addition to the orbital-derived FE polarization of about 6000 μC/m^2—appears in the magnetic phases. In contrast, in GeV_4S_8, the magnetically ordered phase shows no excess but rather a reduction of polarization (*31*). In the remaining part of this article, we focus on the most important and fascinating aspect of these results, namely, the multiferroic nature of the different magnetically ordered phases, including the SkL phase, where skyrmions are dressed with local FE polarization. Specifically, it seems important to clarify the origin of excess polarizations, which will be performed in the theoretical section (Microscopic origin of spin-driven polarization).

Phase diagram of GaV_4S_8

Figure 2 presents the phase diagram of GaV_4S_8 based on magnetization, magnetocurrent, and pyrocurrent, as well as on measurements of specific heat for magnetic fields applied along the crystallographic ⟨111⟩ direction [a phase diagram based on magnetization measurements alone has been published by Kézsmárki *et al.* (*9*)]. In GaV_4S_8, owing to easy-axis exchange anisotropy, the skyrmion cores are always aligned parallel to the ⟨111⟩ easy axis and are not oriented by low external magnetic fields. Therefore, when the magnetic field is applied along

the ⟨111⟩ direction, one magnetically favorable domain coexists with three unfavorable domains, whose cycloidal and SkL states persist up to higher fields (*9*). The finite electric polarization measured without poling electric fields indicates unequal domain population. Moreover, because its value does not change after several warming-cooling cycles, we assume that a unique domain (that is, essentially a monodomain polarization) is stabilized in the present experiment. Therefore, Fig. 2 focuses on the low-field phase diagram specific for this domain, neglecting the cycloidal and SkL phases occurring at higher fields in the magnetically unfavorable domains (*9*).

Figure 2A presents the magnetic field–versus–temperature phase diagram of GaV_4S_8 for $T < 15$ K, whereas Fig. 2B shows the complete H-T phase diagram extending beyond the Jahn-Teller transition. Below the magnetic phase transition occurring at $T_C = 12.7$ K, two magnetic phase pockets (the cycloidal and SkL phases) are embedded in the FM phase (*9*). In zero magnetic field, the FM, cycloidal, and orbitally ordered paramagnetic (PM) phases are all FE, as evidenced by Fig. 1B (denoted as FE2, FE3, and FE1, respectively, in Fig. 2). The orbitally disordered phase above $T_{JT} = 44$ K is a PM semiconductor without FE polarization.

For further elucidation of the phase diagram (Fig. 2A), a representative set of magnetization, specific heat, and polarization curves as a function of temperature and magnetic field is shown in Fig. 3. At the phase boundaries, clear anomalies can be identified in the field-dependent (Fig. 3, A, C, and E) and temperature-dependent (Fig. 3, B, D, and F) scans of all three quantities. The only exception is the temperature dependence of heat capacity (Fig. 3D), which reveals no anomaly when passing from the cycloidal phase to the FM phase. This may be attributed to the fact that the entropy change between the cycloidal state and the FM state is expected to be very small as a result of the long wavelength of the cycloid. The positions of all observed anomalies are included in Fig. 2A, in perfect agreement with each other and with published phase boundaries (*9*), and thus convincingly document the complexity of the low-temperature phase diagram of GaV_4S_8, including a relatively extended SkL phase which reveals spontaneous FE polarization. The excess spin-driven polarization ΔP at the magnetic phase boundaries, as presented in Fig. 3 (E and D), appears on top of a much larger orbital order–derived polarization (Fig. 1B).

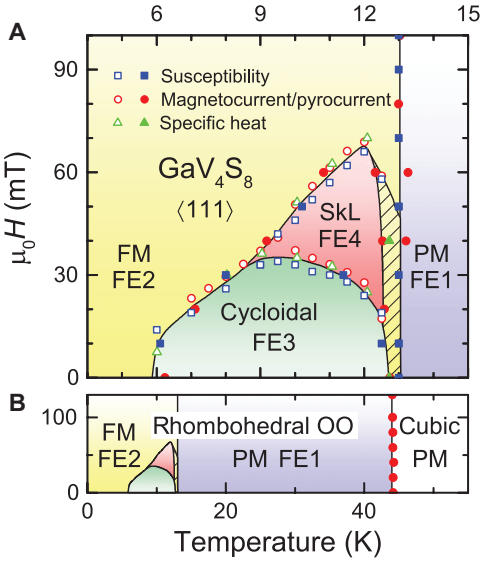

Fig. 2. Magnetic field–versus–temperature phase diagram of GaV_4S_8 for magnetic fields applied along one of the cubic ⟨111⟩ axes. (**A**) Low-temperature region below $T = 15$ K. The magnetic phase boundaries correspond to the unique structural domain whose easy axis is parallel to the magnetic field (for details, see the text). The SkL phase (red area) and the cycloidal phase (green area) are embedded within the FM phase (yellow area). Above $T_C = 12.7$ K, the material is PM. The phase boundaries, as determined from measurements of magnetization, polarization (pyrocurrent and magnetocurrent), and specific heat, are indicated by squares, circles, and triangles, respectively. Full symbols correspond to temperature scans, whereas open symbols represent magnetic field scans. The hatched area characterizes the regime between the PM phase and the cycloidal/SkL phase, where the exact spin structure is unknown. (**B**) Complete phase diagram extending beyond the Jahn-Teller transition. Below T_{JT}, within the orbitally ordered (OO) phase, four different FE states (FE1 to FE4) are found, each characterized by well-distinguishable polarization.

Ferroelectricity in magnetic phases

To obtain more detailed information about the different FE phases, including the SkL phase, we studied the temperature dependence (Fig. 4) and field dependence (Fig. 5) of FE polarization deduced from pyrocurrent and magnetocurrent measurements, respectively. All scans presented in Figs. 3 to 5 show only the excess polarizations in the magnetic phases, which are less than 2% of the orbitally derived ferroelectricity emerging at T_{JT} (inset to Fig. 1B).

Figure 4 shows the temperature dependence of the excess polarization ΔP in various magnetic fields between 0 and 100 mT, whereas Fig. 5 presents polarization versus magnetic field at various temperatures between 2 and 13 K. The steps observed in the field dependence and temperature dependence of the polarization, corresponding to peaks in the magnetocurrent and pyrocurrent curves, are indicated in Fig. 2A by open and full circles, respectively. They nicely match the phase boundaries determined from data on specific heat and magnetization (fig. S1). All magnetically ordered phases are characterized by different excess polarizations. In fields of $\mu_0 H = 100$ mT, the material undergoes a PM-to-FM transition at $T_C = 12.7$ K without any intermediate phase, and the excess polarization in the FM phase reaches the saturation value $\Delta P_{FM} \sim 86\ \mu C/m^2$ at the lowest temperatures (Fig. 4). The curves measured in $\mu_0 H = 0$ and 20 mT, after a steep increase at 13 K, exhibit an additional drop at about 6 K, where the transition from the cycloidal phase to the FM phase takes place (Fig. 2). Therefore, the polarization in the cycloidal phase is enhanced by about 14 $\mu C/m^2$ compared to the purely FM collinear spin arrangement, resulting in a total excess polarization $\Delta P_{cyc} \sim 100\ \mu C/m^2$. The SkL phase–to–FM phase boundary is also accompanied by small but significant anomalies, as revealed by the polarization curves measured in $\mu_0 H = 40$ and 60 mT (Fig. 4). The scan at 40 mT, only crossing the SkL state between 8 and 13 K, reveals an extra contribution of about 5 $\mu C/m^2$, resulting in an excess polarization $\Delta P_{SkL} \sim 91\ \mu C/m^2$ for the SkL phase. Indeed, in Fig. 5, the magnetic field–dependent polarization curves recorded at temperatures between 10 and 12 K show two subsequent steps proving that the cycloidal, SkL, and FM phases exhibit different excess polarizations. This hierarchy of polarization also becomes evident from the isothermal scans in Fig. 5: At $T = 10.5$ K and for increasing magnetic fields, the polarization drops from about 87 $\mu C/m^2$ in the cycloidal phase to 82 $\mu C/m^2$ in the SkL phase and, finally, to 73 $\mu C/m^2$ in the FM state.

It is interesting to compare the spin-derived polarization in the Néel-type skyrmion host GaV_4S_8 with that observed in Cu_2OSeO_3 with Bloch-type skyrmions. In Cu_2OSeO_3, which is so far the only insulating

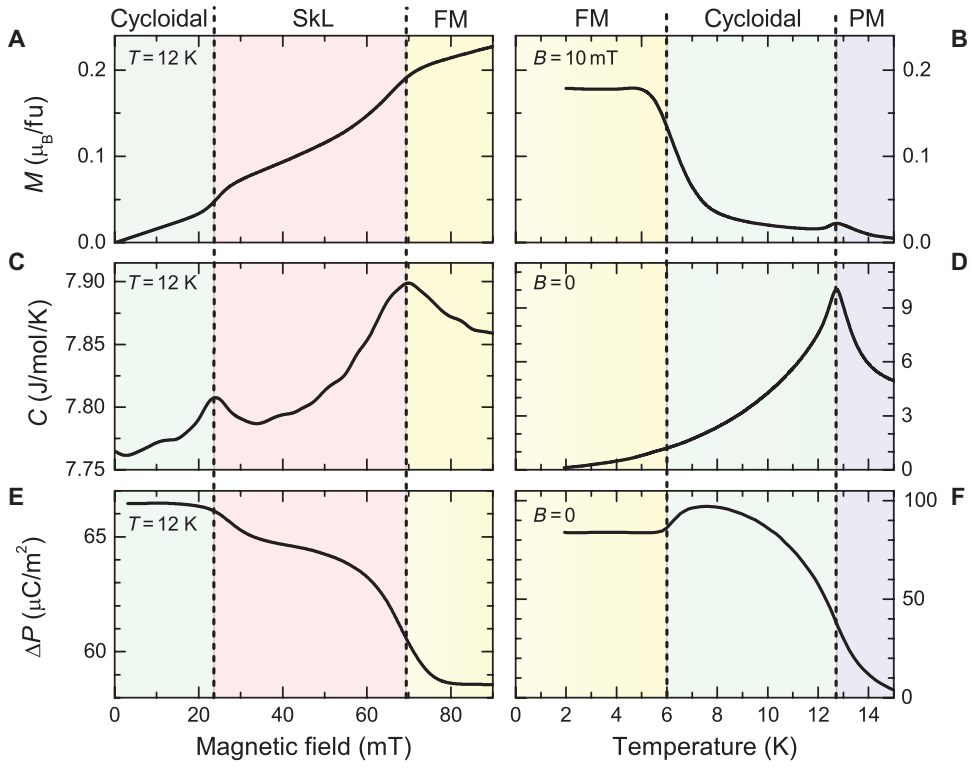

Fig. 3. Anomalies in magnetization, specific heat, and FE polarization at the magnetic phase boundaries. (**A**, **C**, and **E**) Magnetic field dependence of magnetization (*M*) given per formula unit (fu), specific heat (*C*), and isothermal polarization (Δ*P*) with $\boldsymbol{H}\|\langle 111\rangle$. (**B**, **D**, and **F**) Temperature dependence of magnetization, specific heat, and zero-field polarization. Background colors represent the different magnetic phases (following the color code used in Fig. 2). fu, definition.

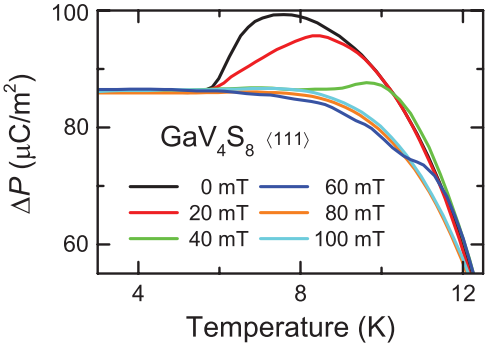

Fig. 4. FE polarization of GaV_4S_8 determined from pyrocurrent measurements. Polarization as a function of temperature measured in various magnetic fields between 0 and 100 mT. Only the excess polarization Δ*P* arising upon entry to the magnetic phases at T_C = 12.7 K is shown.

material reported to host an SkL state, the polarization varies within the range of ±0.5 μC/m^2 in the helical and SkL phases (*8*, *47*, *48*). This is significantly lower than the polarizations observed in the lacunar spinel compound investigated in the present study. Another important difference is that, although FE polarization continuously increases with increasing external magnetic field and is zero for zero magnetic field in the helical and FM phases of Cu_2OSeO_3 (*8*), well-developed excess polarization plateaus are detected in all magnetic phases of GaV_4S_8 even in the absence of external magnetic fields (Fig. 5). This fact demonstrates that the excess polarization in GaV_4S_8 is spin-driven and spontaneously appears at the magnetic phase boundaries, whereas the polarization in Cu_2OSeO_3 is induced by external magnetic fields only and follows a quadratic magnetoelectric coupling (*8*).

Microscopic origin of spin-driven polarization

Motivated by the distinct values of spin-driven polarization in the cycloidal, SkL, and FM phases, we analyze its microscopic origin by taking into account the rhombohedral symmetry of the lattice and the spin patterns in the three magnetically ordered phases. The building blocks of the magnetic structure, the V_4 tetrahedra with S = ½, form an fcc lattice that is elongated parallel to one of the ⟨111⟩ axes. Because of this distortion, the bonds between nearest-neighbor V_4 units within the (111) planes are not equivalent to those connecting V_4 units in neighboring (111) planes, as illustrated in Fig. 6. Hereafter, these bonds are referred to as intraplane and interplane bonds, respectively.

In general, the spin-driven excess polarization Δ*P* can be written as the sum of the polarizations of individual bonds as a bilinear function of spin components

$$\Delta P^{\alpha} = \frac{1}{N} \sum_{\substack{\langle i,j \rangle \\ \beta,\gamma}} \lambda_{i,j}^{\alpha\beta\lambda} S_i^{\beta} S_j^{\gamma} \qquad (1)$$

where the summation goes over all β and γ spin components for each ⟨*i*, *j*⟩ bond. Because GaV_4S_8 is an S = ½ cluster-spin system and because orbital degeneracy is lifted by rhombohedral distortion, the on-site ($i = j$)

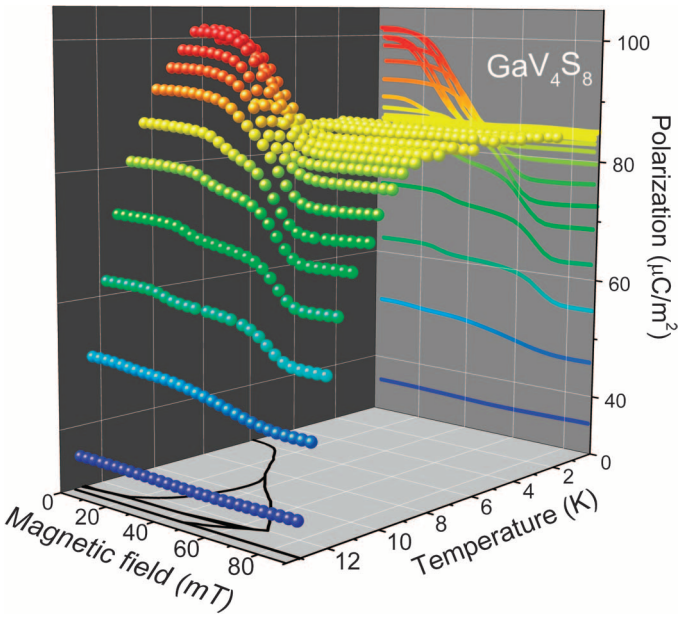

Fig. 5. FE polarization of GaV_4S_8 determined from magnetocurrent measurements. Magnetic field dependence of isothermal polarization measured at various temperatures between 2 and 13 K. Only the excess polarization ΔP induced by magnetic ordering is shown. A step-like increase in polarization at the transition from the cycloidal phase to the SkL phase and from the SkL phase to the FM phase can be identified in the *P*(*H*) curves measured between 7 and 12.5 K. All of the *P*(*H*) curves are projected onto the *H*-*P* plane, and all phase boundaries are indicated on the *H*-*T* plane. The black lines on the *H*-*T* plane indicate the same magnetic phase boundaries as in Fig. 2A.

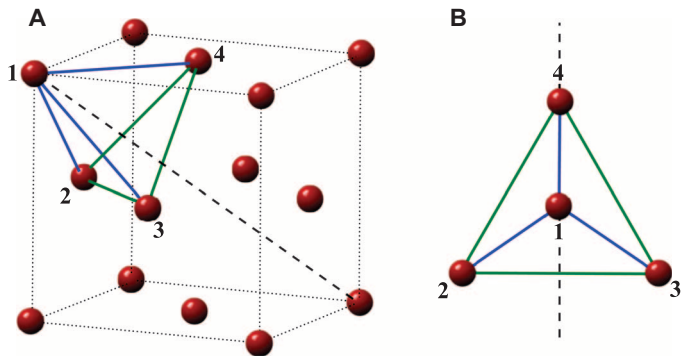

Fig. 6. Bond symmetry in the rhombohedrally distorted structure of GaV_4S_8. (**A**) V_4 clusters (red spheres) form an fcc lattice that is stretched along one of the body diagonals (dashed line). Two types of bonds result from this distortion, as illustrated for four selected clusters: intraplane bonds (green lines) between nearest-neighbor V_4 units within the (111) planes and interplane bonds (blue lines) connecting V_4 units in neighboring (111) planes. (**B**) The four selected clusters viewed from the ⟨111⟩ direction. Each blue bond lies within a mirror plane of the tetrahedron (see dashed line for an example), whereas green bonds are perpendicular to them.

polarization terms can be neglected in the first order. The form of the magnetoelectric coupling tensors $\lambda_{i,j}^{\alpha\beta\lambda}$ is bond-specific and dictated by the symmetry of the bonds (*49*, *50*). In the experiment, only ΔP^z was detected, where the *z* axis points along the ⟨111⟩ direction. Hence, we will restrict our analysis to the second-rank tensors $\lambda_{i,j}^{(z)\beta\lambda}$ and will omit the *z* index. (Because of the presence of FE polarization in the PM phase, $\lambda_{i,j}^{\beta\lambda}$ has the same form, that is, the same independent nonzero elements, as the exchange coupling matrix $J_{i,j}^{\beta\lambda}$). As shown in Fig. 6, intraplane bonds are perpendicular to the mirror planes present in the C_{3v} symmetry, whereas interplane bonds lie within these mirror planes. Correspondingly, the magnetoelectric coupling tensors for selected intraplane and interplane bonds in Fig. 6B have the forms

$$\hat{\lambda}_{2,3} = \begin{bmatrix} \lambda^{xx} & \lambda^{xy} & \lambda^{xz} \\ -\lambda^{xy} & \lambda^{yy} & \lambda^{yz} \\ -\lambda^{xz} & \lambda^{yz} & \lambda^{zz} \end{bmatrix} \quad \hat{\lambda}_{1,4} = \begin{bmatrix} \Lambda^{xx} & 0 & 0 \\ 0 & \Lambda^{yy} & \Lambda^{yz} \\ 0 & \Lambda^{zy} & \Lambda^{zz} \end{bmatrix} \tag{2}$$

The symmetric and antisymmetric parts of the tensors describe the polarization generated by the exchange striction and spin-current mechanisms, respectively (*44*, *49*, *51*). The form of $\hat{\lambda}$ matrices for the other bonds can be derived by applying threefold rotations.

Next, we calculate the uniform component of ΔP_z in the magnetically ordered phases using the magnetoelectric coupling tensors described in Eq. 2. Because the wavelength of magnetic modulation ($2\pi/q$) is more than 20 times larger than the lattice constant *a* in both cycloidal and SkL phases (*9*), we use the continuum approximation when describing their spin patterns

$$\mathbf{S}_{\mathrm{cyc}}(\mathbf{r}) = \frac{1}{2}\left[a_1 \Re\left\{\mathbf{S}_j e^{i\mathbf{q}_j\mathbf{r}}\right\} + \text{higher harmonics}\right] \tag{3a}$$

$$\mathbf{S}_{\mathrm{SkL}}(\mathbf{r}) = \frac{1}{2}\left[b_0\mathbf{S}_0 + b_1\sum_{j=1}^{3}\Re\left\{\mathbf{S}_j e^{i\mathbf{q}_j\mathbf{r}}\right\} + \text{higher harmonics}\right] \tag{3b}$$

$$\mathbf{S}_{\mathrm{FM}}(\mathbf{r}) = \frac{1}{2}c_0\mathbf{S}_0 \tag{3c}$$

where the propagation vectors of magnetic order are $\mathbf{q}_1 = q(1, 0, 0)$, $\mathbf{q}_2 = q\left(-\frac{1}{2}, \frac{\sqrt{3}}{2}, 0\right)$, and $\mathbf{q}_3 = q\left(-\frac{1}{2}, -\frac{\sqrt{3}}{2}, 0\right)$, and the corresponding Fourier components are $\mathbf{S}_j = \mathbf{S}_0 - i\mathbf{q}_j/q$ with $\mathbf{S}_0 = (0,0,1)$. In zero magnetic field, we assume that the cycloid has only the fundamental harmonic (that is, $a_i = 0$ for $i > 0$), which is valid when the magnetic anisotropy is small. The SkL can also be expressed as a Fourier series, where each order contains a superposition of three cycloids whose $\mathbf{q}$ vectors sum up to zero. In the first order, these are the three fundamental harmonics with $\mathbf{q}_1$, $\mathbf{q}_2$, and $\mathbf{q}_3$. Higher-order terms are necessary to keep the spin length constant. The coefficients a_j, b_j, and c_0 depend on the temperature and magnetic field. The uniform component of the polarization can be directly obtained by substituting Eqs. 2 and 3 into Eq. 1 and by integrating over the area of the magnetic unit cell of the respective phases

$$\Delta P_{\mathrm{cyc}} \approx \frac{3}{16}\,a_1^2\left[(\lambda^{zz} + \Lambda^{zz}) + \sum_{\alpha}(\lambda^{\alpha\alpha} + \Lambda^{\alpha\alpha})\right] \tag{4a}$$

$$\Delta P_{\mathrm{SkL}} \approx \frac{3}{4}\,b_0^2(\lambda^{zz} + \Lambda^{zz}) + \frac{9}{16}\sum_{i=1} b_i^2\left[(\lambda^{zz} + \Lambda^{zz}) + \sum_{\alpha}(\lambda^{\alpha\alpha} + \Lambda^{\alpha\alpha})\right] \tag{4b}$$

$$\Delta P_{\mathrm{FM}} \approx \frac{3}{4}\,c_0^2(\lambda^{zz} + \Lambda^{zz}) \tag{4c}$$

All of the polarization terms above come from the exchange striction mechanism. We assume that contributions from the spin-current mechanism, corresponding to the asymmetric parts of the $\hat{\lambda}$ matrices, can be neglected even in the noncollinear cycloidal and SkL phases because of the slow spatial variation of these magnetic patterns. Additional contributions to the polarization arising from higher harmonics in the cycloidal and SkL states are governed by the strength of the weak exchange anisotropy $\frac{\delta J}{J} = \frac{2(J^{zz} - J^{xx})}{J^{xx} + J^{zz}} \approx 0.05$ (that is, reduced by the factor of $\delta J/J$ relative to the leading terms in Eqs. 4a and 4b).

Reflecting the axial symmetry in the rhombohedral phase, the polarization in leading order can be expressed by two parameters of the $\hat{\lambda}$ matrices, namely, the sum of their zz elements, $(\lambda^{zz} + \Lambda^{zz})$, and the sum of their traces, $\sum_{\alpha}(\lambda^{\alpha\alpha} + \Lambda^{\alpha\alpha})$. Next, we determine these parameters based on the measured excess polarizations of the cycloidal and FM phases, assuming that the ordered moment in the FM ground state and the low-temperature region of the cycloidal phase is close to $S = ½$ (that is, $a_1 \approx c_0 \approx 1$). With $\Delta P_{cyc} = 100\ \mu C/m^2$ and $\Delta P_{FM} = 86\ \mu C/m^2$, we obtain $(\lambda^{zz} + \Lambda^{zz}) = 115\ \mu C/m^2$ and $\sum_{\alpha}(\lambda^{\alpha\alpha} + \Lambda^{\alpha\alpha}) = 418\ \mu C/m^2$. Detailed descriptions of the spin structure in the SkL phase (that is, the exact values of the b_n coefficients in Eq. 4b) are not available; thus, for visualization of the spatial dependence of the FE polarization associated with the spin structure of a Néel-type skyrmion, we use the following model of a single skyrmion (*52*)

$$\mathbf{S}_{Sk}(\mathbf{r}) = \frac{1}{2}\begin{bmatrix} \frac{2\xi x}{x^2 + y^2 + \xi^2} \\ \frac{2\xi y}{x^2 + y^2 + \xi^2} \\ \frac{x^2 + y^2 - \xi^2}{x^2 + y^2 + \xi^2} \end{bmatrix} \quad (5)$$

where ξ is the effective radius of the skyrmion core. At this radius, the z component of the spins changes sign when moving from the center to the edge of the skyrmion. The spatial dependence of the z component of the spin-driven polarization reads as

$$\Delta P_{Sk} \approx \frac{3}{2}\left[\frac{4\xi^2(x^2 + y^2)}{(x^2 + y^2 + \xi^2)^2}\frac{\lambda^{xx} + \Lambda^{xx} + \lambda^{yy} + \Lambda^{yy}}{2} + \frac{(x^2 + y^2 - \xi^2)^2}{(x^2 + y^2 + \xi^2)^2}(\lambda^{xx} + \Lambda^{xx})\right] \quad (6)$$

Figure 7 shows the corresponding spatial dependence of the z component of the spin and the polarization. For the magnitude of the magnetoelectric coefficients $\hat{\lambda}$ in Eq. 6, we use the values determined above from the analysis of the cycloidal and FM phases. The characteristic ring-like pattern of the z component of the polarization and its strong spatial modulation in the vicinity of the skyrmion core (as high as 25 to 30%) should allow the experimental verification of this nanoscale polarization pattern accompanying the formation of the Néel-type SkL in multiferroic GaV_4S_8.

DISCUSSION

Here, we have identified four different FE phases in the magnetic semiconductor GaV_4S_8. The large polarization (about 6000 $\mu C/m^2$) in the FE1 phase, which appears below the Jahn-Teller transition, likely originates from a combination of ionic displacements and redistribution of

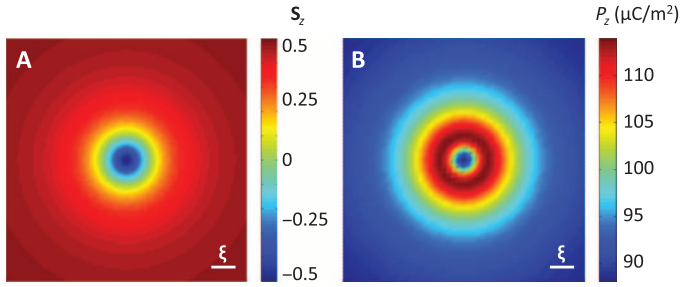

Fig. 7. Polar dressing of SkL in GaV_4S_8. (**A**) Spatial dependence of the z component of the $S = ½$ spins forming the skyrmion and (**B**) spatial dependence of the spin-driven polarization P_z, both on the xy plane perpendicular to the vortex core. The radius of the skyrmion core ξ sets the lateral length scale. The polarization reaches its maximum in a ring-like region around the skyrmion cores (red regions). The outer blue regions in the polarization indicate the FE polarization of the almost collinear spin arrangement at the outer rims of the skyrmion.

electron density driven by the ferro-orbital order and is further enhanced upon entry to the magnetically ordered phases at low temperatures. The excess polarization of the FE2 phase, which is the ground state with a collinear FM order, is about 86 $\mu C/m^2$. The noncollinear spin patterns in the cycloidal and SkL phases further enhance FE polarization, and all multiferroic phases (FE2, FE3, and FE4) can be characterized by three distinct levels of the excess polarization. Although the term "multiferroic" often refers to the coexistence of ferroelectricity and ferromagnetism only, as realized in the FE2 phase, it is generally used in a broader sense to include more common classes of FE materials with antiferromagnetic or ferrimagnetic order, such as the FE3 and FE4 phases of GaV_4S_8. The four FE phases, three of which are also magnetically ordered, point to a complex entanglement of charge, orbital, and magnetic degrees of freedom in the lacunar spinel GaV_4S_8. We observe magnetic skyrmions with additional spin-driven ferroelectricity. Model calculations indicate a strong spatial modulation of FE polarization in the vicinity of the skyrmion core. This donut-shaped polar structure is shown in Fig. 7B.

We argue that the spin-driven polarization is dominated by the exchange striction mechanism in each multiferroic phase: (i) the spin-dependent orbital hybridization mechanism plays a minor role as a result of the $S = ½$ spins of the V_4 clusters, whereas (ii) the spin-current mechanism is inefficient owing to the slow spatial variation of the spin patterns. The latter means that the Dzyaloshinskii-Moriya interaction generally required for the formation of the SkL phase does not significantly contribute to the magnetically induced FE polarization in GaV_4S_8. We have studied the origin of magnetoelectric effect at the microscopic level by analyzing the symmetry of V_4–V_4 bonds in the rhombohedral phase and have determined the two sets of magnetoelectric coefficients responsible for the spin-driven polarization.

The excess polarization in the SkL phase of GaV_4S_8 is almost two orders of magnitude larger than that of Cu_2OSeO_3, the only magnetoelectric skyrmion-host material known so far. There is no spontaneous FE polarization in the latter material; the polarization is only induced by external magnetic fields. The sizable polarization in GaV_4S_8 may offer an efficient electric control of the SkL state, as already demonstrated in Cu_2OSeO_3 (*12*, *13*), which would be an important step toward the development of skyrmion-based memory devices (*3*, *5*, *18*, *53*). This ambitious goal requires, at the first stage, nanoscale observations of

the polar pattern associated with the SkL, using local probes such as scanning force microscopy and Kelvin probe microscopy (*54*–*56*).

MATERIALS AND METHODS

Polycrystalline GaV_4S_8 was prepared by solid-state reaction using pure elements of Ga (6N), V (3N), and S (5N). Three subsequent synthesis steps were necessary to obtain the full reaction of the starting materials for the formation of the stoichiometric ternary phase. Phase purity after each step was checked by x-ray powder diffraction. The synthesized polycrystals were used as starting material for single crystal growth, using chemical transport reactions. Growth occurred in closed quartz ampoules at temperatures between 800 and 850°C, with iodine as transport agent. Crushed single crystals were characterized by x-ray diffraction and found to be free of any impurities. At room temperature, the correct $GaMo_4S_8$-type structure with F_{43m} symmetry and a lattice constant $a = 0.966$ nm were found. Magnetic measurements were performed using an MPMS XL SQUID magnetometer (Quantum Design) in the temperature range $1.8\ K < T < 400\ K$ and in external magnetic fields up to 5 T. Heat capacity was investigated using a Physical Properties Measurement System (Quantum Design) for temperatures $1.8\ K < T < 300\ K$. Dielectric experiments were performed using a Novocontrol Alpha Analyzer (frequency range, 1 Hz to 10 MHz) and an Agilent E4991A impedance analyzer (frequency range, 1 MHz to 3 GHz). The pyrocurrent was measured using the Keithley Electrometer 6517A (Keithley Instruments) as a function of temperature between 2 and 55 K. In addition, we measured the magnetocurrent at temperatures between 2 and 14 K and in external fields between 0 and 300 mT. In these experiments, we used platelet-shaped single crystals (size, 1 mm^2; thickness, 0.25 mm). The large (111) surfaces of these samples were contacted by silver paste.

SUPPLEMENTARY MATERIALS

Supplementary material for this article is available at http://advances.sciencemag.org/cgi/content/full/1/10/e1500916/DC1

Sample characterization

Fig. S1. Sample characterization.

Hysteresis at the Jahn-Teller transition

Fig. S2. Hysteresis behavior of magnetic susceptibility.

Fig. S3. Hysteresis behavior of dielectric constant.

Maxwell-Wagner relaxation and intrinsic dielectric response

Fig. S4. Dielectric constant up to 300 K.

Determination of the ferroelectric polarization

References (*57*, *58*)

REFERENCES AND NOTES

1. U. K. Rößler, A. N. Bogdanov, C. Pfleiderer, Spontaneous skyrmion ground states in magnetic metals. *Nature* **442**, 797–801 (2006).
2. S. Mühlbauer, B. Binz, F. Jonietz, C. Pfleiderer, A. Rosch, A. Neubauer, R. Georgii, P. Böni, Skyrmion lattice in a chiral magnet. *Science* **323**, 915–919 (2009).
3. A. Fert, V. Cros, J. Sampaio, Skyrmions on the track. *Nat. Nanotechnol.* **8**, 152–156 (2013).
4. N. Romming, C. Hanneken, M. Menzel, J. E. Bickel, B. Wolter, K. von Bergmann, A. Kubetzka, R. Wiesendanger, Writing and deleting single magnetic skyrmions. *Science* **341**, 636–639 (2013).
5. N. Nagaosa, Y. Tokura, Topological properties and dynamics of magnetic skyrmions. *Nat. Nanotechnol.* **8**, 899–911 (2013).
6. P. Milde, D. Köhler, J. Seidel, L. M. Eng, A. Bauer, A. Chacon, J. Kindervater, S. Mühlbauer, C. Pfleiderer, S. Buhrandt, C. Schütte, A. Rosch, Unwinding of a skyrmion lattice by magnetic monopoles. *Science* **340**, 1076–1080 (2013).
7. C. Schütte, A. Rosch, Dynamics and energetics of emergent magnetic monopoles in chiral magnets. *Phys. Rev. B* **90**, 174432 (2014).
8. S. Seki, X. Z. Yu, S. Ishiwata, Y. Tokura, Observation of skyrmions in a multiferroic material. *Science* **336**, 198–201 (2012).
9. I. Kézsmárki, S. Bordács, P. Milde, E. Neuber, L. M. Eng, J. S. White, H. M. Rønnow, C. D. Dewhurst, M. Mochizuki, K. Yanai, H. Nakamura, D. Ehlers, V. Tsurkan, A. Loidl, Néel-type skyrmion lattice with confined orientation in the polar magnetic semiconductor GaV_4S_8. *Nat. Mater.* **14**, 1116–1122 (2015).
10. M. Fiebig, Revival of the magnetoelectric effect. *J. Phys. D Appl. Phys.* **38**, R123–R152 (2005).
11. N. A. Spaldin, M. Fiebig, The renaissance of magnetoelectric multiferroics. *Science* **309**, 391–392 (2005).
12. J. S. White, I. Levatić, A. A. Omrani, N. Egetenmeyer, K. Prša, I. Živković, J. L. Gavilano, J. Kohlbrecher, M. Bartkowiak, H. Berger, H. M. Rønnow, Electric field control of skyrmion lattice in Cu_2OSeO_3. *J. Phys. Condens. Matter* **24**, 432201 (2012).
13. J. S. White, K. Prša, P. Huang, A. A. Omrani, I. Živković, M. Bartkowiak, H. Berger, A. Magrez, J. L. Gavilano, G. Nagy, J. Zang, H. M. Rønnow, Electric-field-induced Skyrmion distortion and giant lattice rotation in the magnetoelectric insulator Cu_2OSeO_3. *Phys. Rev. Lett.* **113**, 107203 (2014).
14. P. Chu, Y. L. Xie, Y. Zhang, J. P. Chen, D. P. Chen, Z. B. Yan, J.-M. Liu, Real-space anisotropic dielectric response in a multiferroic skyrmion lattice. *Sci. Rep.* **5**, 8318 (2015).
15. T. Schulz, R. Ritz, A. Bauer, M. Halder, M. Wagner, C. Franz, C. Pfleiderer, K. Everschor, M. Garst, A. Rosch, Emergent electrodynamics of skyrmions in a chiral magnet. *Nat. Phys.* **8**, 301–304 (2012).
16. J. Zang, M. Mostovoy, J. H. Han, N. Nagaosa, Dynamics of skyrmion crystals in metallic thin films. *Phys. Rev. Lett.* **107**, 136804 (2011).
17. M. Onoda, G. Tatara, N. Nagaosa, Anomalous Hall effect and skyrmion number in real and momentum spaces. *J. Phys. Soc. Jpn.* **73**, 2624–2627 (2004).
18. M. Mochizuki, X. Z. Yu, S. Seki, N. Kanazawa, W. Koshibae, J. Zang, M. Mostovoy, Y. Tokura, N. Nagaosa, Thermally driven ratchet motion of a skyrmion microcrystal and topological magnon Hall effect. *Nat. Mater.* **13**, 241–246 (2014).
19. H. Barz, New ferromagnetic molybdenum spinels. *Mater. Res. Bull.* **8**, 983–988 (1973).
20. C. Perrin, M. R. Chevrel, M. Sergent, New tetrahedral clusters of molybdenum in chalcogenides MMo_4S_8 (M=Al,Ga), $GaMo_4Se_8$ and thiohalides MoSX (X=Cl, Br, I). *C. R. Acad. Sci. Paris* **280**, 949–951 (1975).
21. D. Brasen, J. M. Vandenberg, M. Robbins, R. H. Willens, W. A. Reed, R. C. Sherwood, X. J. Pinder, Magnetic and crystallographic properties of spinels of the type $A_xB_2S_4$ where A = Al, Ga, and B = Mo, V, Cr, *J. Solid State Chem.* **13**, 298–303 (1975).
22. H. Müller, W. Kockelmann, D. Johrendt, The magnetic structure and electronic ground states of Mott insulators GeV_4S_8 and GaV_4S_8. *Chem. Mater.* **18**, 2174–2180 (2006).
23. M. M. Abd-Elmeguid, B. Ni, D. I. Khomskii, R. Pocha, D. Johrendt, X. Wang, K. Syassen, Transition from Mott insulator to superconductor in $GaNb_4Se_8$ and $GaTa_4Se_8$ under high pressure. *Phys. Rev. Lett.* **93**, 126403 (2004).
24. V. Ta Phuoc, C. Vaju, B. Corraze, R. Sopracase, A. Perucchi, C. Marini, P. Postorino, M. Chligui, S. Lupi, E. Janod, L. Cario, Optical conductivity measurements of $GaTa_4Se_8$ under high pressure: Evidence of a bandwidth-controlled insulator-to-metal Mott transition. *Phys. Rev. Lett.* **110**, 037401 (2013).
25. A. Camjayi, C. Acha, R. Weht, M. G. Rodríguez, B. Corraze, E. Janod, L. Cario, M. J. Rozenberg, First-order insulator-to-metal Mott transition in the paramagnetic 3D system $GaTa_4Se_8$. *Phys. Rev. Lett.* **113**, 086404 (2014).
26. E. Dorolti, L. Cario, B. Corraze, E. Janod, C. Vaju, H.-J. Koo, E. Kan, M.-H. Whangbo, Half-metallic ferromagnetism and large negative magnetoresistance in the new lacunar spinel $GaTi_3VS_8$. *J. Am. Chem. Soc.* **132**, 5704–5710 (2010).
27. H.-S. Kim, J. Im, M. J. Han, H. Jin, Spin-orbital entangled molecular j_{eff} states in lacunar spinel compounds. *Nat. Commun.* **5**, 3988 (2014).
28. V. Dubost, T. Cren, C. Vaju, L. Cario, B. Corraze, E. Janod, F. Debontridder, D. Roditchev, Resistive switching at the nanoscale in the Mott insulator compound $GaTa_4Se_8$. *Nano Lett.* **13**, 3648–3653 (2013).
29. P. Stoliar, L. Cario, E. Janod, B. Corraze, C. Guillot-Deudon, S. Salmon-Bourmand, V. Guiot, J. Tranchant, M. Rozenberg, Universal electric-field-driven resistive transition in narrow-gap Mott insulators. *Adv. Mater.* **25**, 3222–3226 (2013).
30. V. Guiot, L. Cario, E. Janod, B. Corraze, V. Ta Phuoc, M. Rozenberg, P. Stoliar, T. Cren, D. Roditchev, Avalanche breakdown in $GaTa_4Se_{8-x}Te_x$ narrow-gap Mott insulators. *Nat. Commun.* **4**, 1722 (2013).
31. K. Singh, C. Simon, E. Cannuccia, M.-B. Lepetit, B. Corraze, E. Janod, L. Cario, Orbital-ordering-driven multiferroicity and magnetoelectric coupling in GeV_4S_8. *Phys. Rev. Lett.* **113**, 137602 (2014).
32. A. V. Powell, A. McDowall, I. Szkoda, K. S. Knight, B. J. Kennedy, T. Vogt, Cation substitution in defect thiospinels: Structural and magnetic properties of $GaV_{4-x}Mo_xS_8$ ($0 \le x \le 4$). *Chem. Mater.* **19**, 5035–5044 (2007).
33. R. Pocha, D. Johrendt, R. Pöttgen, Electronic and structural instabilities in GaV_4S_8 and $GaMo_4S_8$. *Chem. Mater.* **12**, 2882–2887 (2000).
34. Y. Sahoo, A. K. Rastogi, Evidence of hopping conduction in the V_4-cluster compound GaV_4S_8. *J. Phys. Condens. Matter* **5**, 5953–5962 (1993).
35. C. S. Yadav, A. K. Nigam, A. K. Rastogi, Thermodynamic properties of ferromagnetic Mott-insulator GaV_4S_8. *Phys. B Condens. Matter* **403**, 1474–1475 (2008).

36. H. Nakamura, H. Chudo, M. Shiga, Structural transition of the tetrahedral metal cluster: Nuclear magnetic resonance study of GaV_4S_8. *J. Phys. Condens. Matter* **17**, 6015–6024 (2005).
37. X. Z. Yu, Y. Onose, N. Kanazawa, J. H. Park, J. H. Han, Y. Matsui, N. Nagaosa, Y. Tokura, Real-space observation of a two-dimensional skyrmion crystal. *Nature* **465**, 901–904 (2010).
38. A. O. Leonov, M. Mostovoy, Multiply periodic states and isolated skyrmions in an anisotropic frustrated magnet. *Nat. Commun.* **6**, 8275 (2015).
39. D. Bichler, V. Zinth, D. Johrendt, O. Heyer, M. K. Forthaus, T. Lorenz, M. M. Abd-Elmeguid, Structural and magnetic phase transitions of the V_4-cluster compound GeV_4S_8. *Phys. Rev. B* **77**, 212102 (2008).
40. M. E. Lines, A. M. Glass, *Principles and Applications of Ferroelectric and Related Materials* (Clarendon Press, Oxford, UK, 1996).
41. P. Lunkenheimer, V. Bobnar, A. V. Pronin, A. I. Ritus, A. A. Volkov, A. Loidl, Origin of apparent colossal dielectric constants. *Phys. Rev. B* **66**, 052105 (2002).
42. P. Lunkenheimer, S. Krohns, S. Riegg, S. G. Ebbinghaus, A. Reller, A. Loidl, Colossal dielectric constants in transition-metal oxides. *Eur. Phys. J. Spec. Top.* **180**, 61–89 (2010).
43. T. Kimura, T. Goto, H. Shintani, K. Ishizaka, T. Arima, Y. Tokura, Magnetic control of ferroelectric polarization. *Nature* **426**, 55–58 (2003).
44. S.-W. Cheong, M. Mostovoy, Multiferroics: A magnetic twist for ferroelectricity. *Nat. Mater.* **6**, 13–20 (2007).
45. Y. Tokura, S. Seki, N. Nagaosa, Multiferroics of spin origin. *Rep. Prog. Phys.* **77**, 076501 (2014).
46. W. J. Merz, Double hysteresis loop of $BaTiO_3$ at the Curie point. *Phys. Rev.* **91**, 513–517 (1953).
47. A. Maisuradze, A. Shengelaya, H. Berger, D. M. Djokić, H. Keller, Magnetoelectric coupling in single crystal Cu_2OSeO_3 studied by a novel electron spin resonance technique. *Phys. Rev. Lett.* **108**, 247211 (2012).
48. A. A. Omrani, J. S. White, K. Prša, I. Živković, H. Berger, A. Magrez, Y.-H. Liu, J. H. Han, H. M. Rønnow, Exploration of the helimagnetic and skyrmion lattice phase diagram in Cu_2OSeO_3 using magnetoelectric susceptibility. *Phys. Rev. B* **89**, 064406 (2014).
49. C. Jia, S. Onoda, N. Nagaosa, J. H. Han, Microscopic theory of spin-polarization coupling in multiferroic transition metal oxides. *Phys. Rev. B* **76**, 144424 (2007).
50. T. A. Kaplan, S. D. Mahanti, Canted-spin-caused electric dipoles: A local symmetry theory. *Phys. Rev. B* **83**, 174432 (2011).
51. H. Katsura, N. Nagaosa, A. V. Balatsky, Spin current and magnetoelectric effect in noncollinear magnets. *Phys. Rev. Lett.* **95**, 057205 (2005).
52. S. L. Sondhi, A. Karlhede, S. A. Kivelson, E. H. Rezayi, Skyrmions and the crossover from the integer to fractional quantum Hall effect at small Zeeman energies. *Phys. Rev. B* **47**, 16419–16426 (1993).
53. J. Sampaio, V. Cros, S. Rohart, A. Thiaville, A. Fert, Nucleation, stability and current-induced motion of isolated magnetic skyrmions in nanostructures. *Nat. Nanotechnol.* **8**, 839–844 (2013).
54. F. Saurenbach, B. D. Terris, Imaging of ferroelectric domain walls by force microscopy. *Appl. Phys. Lett.* **56**, 1703–1705 (1990).
55. L. M. Eng, Nanoscale domain engineering and characterization of ferroelectric domains. *Nanotechnology* **10**, 405–411 (1999).
56. S. Kawai, A. S. Foster, F. F. Canova, H. Onodera, S.-I. Kitamura, E. Meyer, Atom manipulation on an insulating surface at room temperature. *Nat. Commun.* **5**, 4403 (2014).
57. V. Malik, C. S. Yadav, A. Rastogi, D. Kumar, Nanoscale domain engineering and characterization of ferroelectric domains. *Europhys. Lett.* **101**, 67008 (2013).
58. L. D. Landau, E. M. Lifshitz, in *Statistical Physics* (Pergamon, Oxford, UK, 1980), chap. XIV.

Acknowledgments

Funding: This research was supported by the Deutsche Forschungsgemeinschaft via the Transregional Research Collaboration TRR 80 "From Electronic Correlations to Functionality" (Augsburg/Munich/Stuttgart) and by the Hungarian Research Funds (OTKA K 108918, OTKA PD 111756, and Bolyai 00565/14/11). **Author contributions:** I.K., A.L., and P.L. conceived and supervised the project. V.T. grew the high-quality single crystals. E.R. performed and analyzed the dielectric measurements. S.W. performed and analyzed the measurements of specific heat. S.B. and I. K. performed the calculations. A.L. wrote the paper with contributions from I.K. and P.L. All authors discussed the results and commented on the manuscript. **Competing interests:** The authors declare that they have no competing interests. **Data and materials availability:** All data needed to evaluate the conclusions in the paper are present in the paper and/or the Supplementary Materials. Additional data related to this paper may be requested from E.R. (eugen.ruff@physik.uni-augsburg.de) or P.L. (peter.lunkenheimer@physik.uni-augsburg.de).

Submitted 10 July 2015
Accepted 10 September 2015
Published 13 November 2015
10.1126/sciadv.1500916

Citation: E. Ruff, S. Widmann, P. Lunkenheimer, V. Tsurkan, S. Bordács, I. Kézsmárki, A. Loidl, Multiferroicity and skyrmions carrying electric polarization in GaV_4S_8. *Sci. Adv.* **1**, e1500916 (2015).

Multiferroicity and skyrmions carrying electric polarization in GaV_4S_8

Eugen Ruff, Sebastian Widmann, Peter Lunkenheimer, Vladimir Tsurkan, Sandor Bordács, Istvan Kézsmárki and Alois Loidl

(November 13, 2015)
Sci Adv 2015, 1:.
doi: 10.1126/sciadv.1500916